Numerical Design of a Micro-LED Based Optogenetic Stimulator for Visual Cortical Prosthesis

Junyu Chen ⓘ, He Ding ⓘ, Ya-tang Li ⓘ, and Xing Sheng ⓘ

Abstract—**Visual impairment represents a critical public health and safety issue, and visual prostheses provide a promising solution to addressing it. Here we present a design strategy for a micro-LED based optogenetic stimulator as visual prosthesis on cortex, and numerically evaluate its performance. First, we provide an introductory overview of visual prostheses, and categorize visual prostheses into four distinct groups based on the stimulation location (retina or visual cortex) and stimulation modality (electrical or optical). Specifically, we focus on the design involving a micro-LED array implanted on the dura mater for visual cortex prosthesis. The study evaluates two optogenetic approaches based on different photosensitive proteins (C1V1 and ChrimsonR) and determines the method of utilizing green light for C1V1 activation. Through comprehensive optical simulations, we optimize the design parameters, and thermal simulations are employed to ensure efficient heat dissipation and tissue safety. The resulting stimulation effects and potential for vision recovery are thoroughly discussed. While challenges associated with tissue scattering and the elucidation of biological visual signal mechanisms impede the efficacy of optical stimulation, further research is warranted to fully harness the potential of visual cortex prostheses and surmount these obstacles.**

Index Terms—**Micro-LED, optogenetics, retina prostheses, visual cortical prostheses.**

I. INTRODUCTION

VISION is one of the most important ways for humans to receive information. The human visual system, which

Manuscript received 21 July 2023; revised 26 October 2023; accepted 8 November 2023. Date of publication 13 November 2023; date of current version 3 January 2024. This work was supported in part by the National Natural Science Foundation of China (NSFC) under Grants 62005016 and 52272277, in part by Beijing Municipal Natural Science Foundation under Grant 4202032, in part by NeuCyber NeuroTech (Beijing) Company Ltd under Grant NC-2023-HE-02, and in part by Beijing Nova Program under Grant 20230484254. *(Corresponding authors: He Ding; Xing Sheng.)*

Junyu Chen and Xing Sheng are with the Department of Electronic Engineering, Beijing National Research Center for Information Science and Technology, Institute for Precision Medicine, Center for Flexible Electronics Technology, and IDG/McGovern Institute for Brain Research, Tsinghua University, Beijing 100084, China (e-mail: cjy22@mails.tsinghua.edu.cn; xingsheng@tsinghua.edu.cn).

He Ding is with the Beijing Engineering Research Center of Mixed Reality and Advanced Display, School of Optics and Photonics, Beijing Institute of Technology, Beijing 100081, China (e-mail: heding@bit.edu.cn).

Ya-tang Li is with the Chinese Institute for Brain Research, Beijing 102206, China (e-mail: yatangli@cibr.ac.cn).

Color versions of one or more figures in this article are available at https://doi.org/10.1109/JSTQE.2023.3332320.

Digital Object Identifier 10.1109/JSTQE.2023.3332320

comprises eyes, the optic nerve, and the brain, is complex and intricate. The eyes first capture light and the retinas convert optical signals into electrical signals through the photoreceptors. Then the signals propagate to retinal ganglion cells (RGCs) and transmitted to the brain via the optic nerve. In the brain, the visual cortex processes these signals and interprets them as visual information, enabling the perception and interpretation of the world [1].

Owing to the intricate nature of the visual system, visual diseases stem from a variety of causative factors, rendering the development of universal treatment modalities a challenging endeavor. For example, gene-replacement therapies that deliver normal gene to the mutated retinal cells have been developed for inherited retinal degenerations [2], [3]. However, the cargo capacity of delivery vectors such as adeno-associated virus (AAV) is lower than most retinal genes and the patients must have surviving photoreceptors, resulting in a limited utility to a narrow range of recessive diseases [1]. Cell-replacement therapies apply degenerated native retinal cells from stem cells to replace damaged or dead cells in the pathological space [4], [5], [6]. Although these methods may be effective for age-related macular degeneration and retinitis pigmentosa, the source of stem cells remains an issue. The autologous method carrying the same genes as patients may lead to disease recurrence, and the allogeneic method faces ethical acceptability and immune compatibility problems. Except the issue of stem cell sources, the transplanted stem cells may not be integrated properly into the existing retinal tissue in patients with advanced disease. Currently, the application fields of these visual restoration methods are relatively restricted and ineffective in treating optic nerve damage caused by glaucoma or any serious disease of the retina, while glaucoma has already become the leading causes of blindness (3.6 million cases in 2020) [7], highlighting the need to develop approaches that target late-stage diseases and possess a high degree of universality.

Utilizing prostheses to directly stimulate components within the visual system presents a potential universal approach towards achieving visual restoration (Fig. 1). Based on the position of stimulation, visual prostheses can be divided into retinal stimulators and cortical stimulators. Electrical stimulation prostheses for retina (Fig. 1(a)) are currently the most mature visual prostheses. The fundamental principle underlying this type of prosthesis involves the conversion of light into electric pulses,

1077-260X © 2023 IEEE. Personal use is permitted, but republication/redistribution requires IEEE permission.
See https://www.ieee.org/publications/rights/index.html for more information.

Authorized licensed use limited to: Tsinghua University. Downloaded on February 11,2024 at 06:07:20 UTC from IEEE Xplore. Restrictions apply.
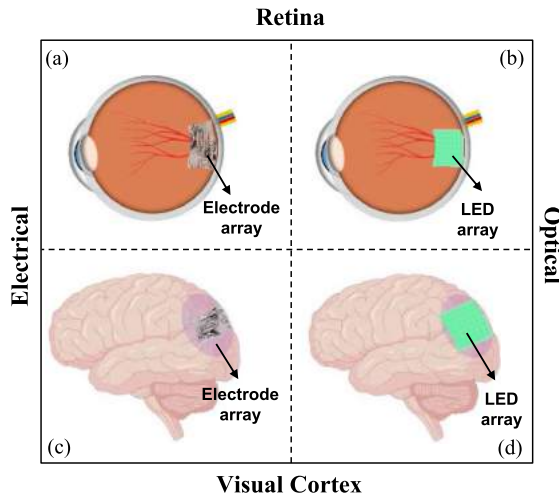
Fig. 1. Schematic illustrations of different visual prosthetic strategies, based on the stimulation modes and locations. (a) Electrical stimulators for retina, (b) LED based optogenetic stimulators for retina, (c) Electrical stimulators for visual cortex and (d) LED based optogenetic stimulators for visual cortex.

which subsequently stimulate the retina. These stimuli are then transmitted via the optic nerves to the brain, facilitating the formation of visual perception. An electrical retina stimulation system is generally composed of a camera to receive external light signals, a power supply and signal conversion module, and a microelectrode array that is implanted into the retina [8]. For example, the Argus II system (the first vision prosthesis to get regulatory approval in the USA and Europe) implants a 60-channel microelectrode array on the posterior pole of the retinal surface to replace photoreceptors [9]. The system uses a portable small processor to convert the picture from the glass-mounted camera to a pixel image and transmits the signals to the microelectrode array through a coil to elicited retinal responses. An alternative electrical retina stimulation strategy uses a photodiode-based electrode array or a nanowire array to replace the microelectrode array [10], [11]. Compared to the first method, this photodiode-based system can directly transfer optical signals into stimulation electrical signals, which means that an external camera may not be needed and people can directly control the images by their eyes. However, weak natural light may cause poor device response and affect the final visual effect. Another commercial product (PRIMA system) adds an external infrared light source to enhance the imaging effect based on this method [12]. The system uses an 880 nm pulsed laser source to convey the images captured and processed by an external camera to an implanted photovoltaic electrode array containing 378 pixels. The photovoltaic electrode transfers the optical signals into electric current to stimulate the inner retinal neurons to form visual signals. Comparing two different electrical stimulation prostheses for retina, they employ various techniques to facilitate the reception of external light signals by the prosthesis and have achieved certain visual restoration effects in some blind patients. The optimal visual acuity achieved by the Argus II is about 20/1200, and the PRIMA achieves about 20/460 [1], [9], [12]. In essence, the current electrical stimulation

retinal prosthesis serves as a substitute for damaged photoreceptors on the retina, aiming to treat conditions characterized by photoreceptors damage such as age-related macular degeneration (AMD) and retinitis pigmentosa (RP).

In addition to electrical stimulation, optical stimulation retinal prostheses (Fig. 1(b)) based on optogenetics provide another option. Optogenetics is a technique that utilizes light-sensitive proteins called opsins to control and manipulate neural activities in central and peripheral systems [13], [14]. In retinal prostheses, optogenetics method transfers light-sensitive genes into photoreceptors or retinal ganglion cells (RGCs) through gene delivery tools like adeno-associated viruses (AAVs). This allows for the expression of light-sensitive pumps or ion channel, enabling cells to be controllable by light. A typical optogenetic visual prosthesis uses thin-film micro-LED array instead of microelectrode array to stimulate RGCs [15]. The wireless, flexible GaN micro-LED array with 8192 pixels and a center wavelength at 545 nm is attached on the retinal surface and can stimulate RGCs expressing ChRmine-mScarlet to evoke visual cortical activity. The device has the ability to create a human visual space of approximately 10 degrees and has achieved the highest pixel count currently available. Another kind of optogenetic retinal prosthesis adopts a strategy similar to the PRIMA [16]. The system consists of a camera and a video processor to capture and simplify image information, a GaN micro-LED array with 8100 pixels emitting light signals and a VR lens. Unlike the first scheme, the micro-LED array is not implanted into the eye, but relies on the VR lens to project light signals onto the retina to active ChR2-expressing cells. The non-implantable design serves to mitigate potential biological damage, however, it also leads to poor visual reconstruction results. Optical stimulation retinal prostheses employ light stimulation to activate neural activity, mitigating biological damage and enhancing spatial resolution. Furthermore, the incorporation of optogenetic techniques facilitates the introduction of light-sensitive proteins into retinal cells, offering potential reparative effects on impaired photoreceptors and RCGs.

Due to the constraint of stimulation location, the utilization of retinal prostheses is primarily applied in photoreceptor diseases like AMD and RP. Prostheses that directly stimulate the visual cortex have been proposed as a potential solution for patients with optic nerve damage (Fig. 1(c)). Primary visual cortex (V1 area) is the first area of cortical processing and receives signals from the eyes. As a crucial part for visual perception and cognition, the V1 region is commonly employed as a stimulus target for visual cortical prostheses. A study that implanted a 1024-channel prosthesis consisting of 16 Utah arrays in V1 and V4 areas of the visual cortex of monkeys has shown the potential of electrical stimulation cortical prostheses in the restoration of the blind [17]. The monkeys can recognize simple shapes or letters under the stimulation of multiple electrodes. Nowadays, a few electrical stimulation cortical prostheses used in humans are in the stage of device development or clinical trials [18]. The Intracortical Visual Prosthesis Project (ICVP) develops a wireless floating microelectrode array system consisting of 144 electrodes with different lengths for intracortical stimulation [19]. Cortical visual neuroprosthesis for the blind

(CORTIVIS) project utilizes Utah electrode array containing 100 narrow electrodes with 1.0–1.5 mm length to excite visual cortex [20]. These systems both adopt intracortical electrodes which can directly stimulate the target area and bring higher spatial resolution, but also increase the risk of tissue damage. Unlike these methods, the Orion system developed based on the Argus II uses 60 surface electrodes to form an electrode grid for subdural stimulation of the visual cortex [18]. The subdural stimulation model enhances the safety but limits the resolution [17]. How to balance the trade-off between reducing implant damage and enhancing spatial resolution has become a challenge for electrical stimulation cortex prostheses. Moreover, electrical based cortical stimulation may introduce additional risks to the patients, such as inducing seizure events and transient headaches [21], [22].

Similar to retinal prostheses, optogenetics also can be applied into cortical prostheses (Fig. 1(d)). An LED array implanted under the dura matter on the visual cortex has been developed for high-throughput optogenetic stimulation [23]. The array comprises 24 LEDs, each emitting light at a center wavelength of 530 nm for C1V1 stimulation. The LEDs have a size of 0.5 mm and are spaced apart at an interval of 1 mm. This device enables optogenetic stimulation at a target depth of 1 mm within the visual cortex and has been demonstrated to exert modulatory effects on visual responses in large primates through behavioral experiments. This prosthetic strategy directly mounts the flexible LED array on the dura and potentially avoids tissue damage to the cerebral cortex by using light as the stimulus, providing a new option for visual cortical prostheses.

Currently, a comprehensive evaluation reveals that each of the four types of visual prostheses possesses unique merits and drawbacks. In terms of stimulation location, retinal prostheses primarily address impairments in the sensory receptors, while visual cortex prostheses hold promise for addressing blindness caused by optic nerve damage such as glaucoma. As for stimulation modality, electrical approaches demonstrate better maturity and offer direct stimulation, whereas optogenetic methods exhibit reduced potential for tissue trauma. In this paper, we focused on optogenetic-based stimulation cortical prostheses, for which existing devices suffer from limitations such as a limited number of channels and low resolution, hindering their ability to support vision restoration. We plan to design an implantable flexible optical visual cortical prosthesis based on micro-LED arrays, and validate the viability of this solution through optical and thermal simulations.

II. RESULTS

To design a micro-LED array for optogenetics-based cortex prostheses, we first need to establish a suitable biological model. In the visual transmission pathway of humans, the optical nerve signal is initially transmitted to the L4 region of V1, which has the highest concentration of nerves within the primary visual cortex [24], [25]. Hence, the L4 area is designated as the targeted region for stimulation. In order to fully exploit the advantages of the light stimulation method and minimize potential biological damage, we propose placing the micro-LED array outside the
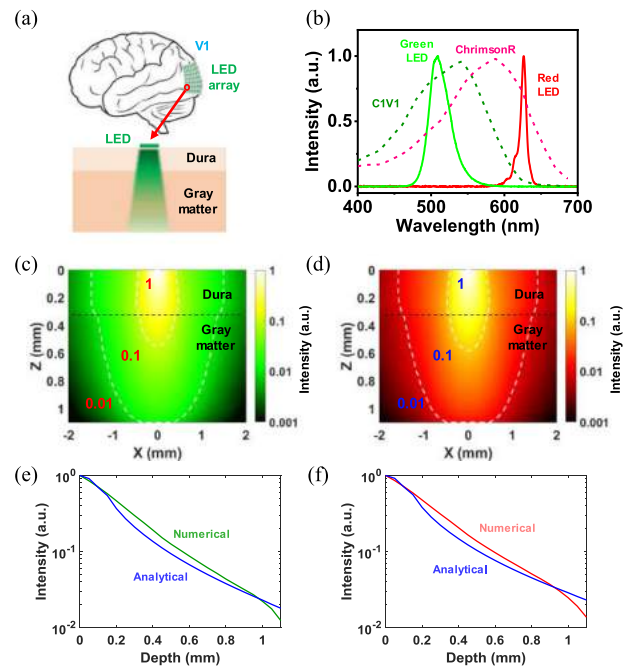

Fig. 2. (a) Optical model showing optogenetic stimulation of the human visual cortex (V1) with surface mounted micro-LEDs. (b) Absorption spectra of ChrimsonR and C1V1, and emission spectra of red and green micro-LEDs. (c) and (d) Normalized light intensity distribution profiles on a cross-sectional plane along the propagation direction based on numerical simulation at wavelengths of (c) 530 nm and (d) 620 nm. (e) and (f) Normalized light intensity profiles at varied depths along the propagation direction at (e) 530 nm and (f) 620 nm.

dura mater. The resulting biological model is a double-layer structure composed of the dura mater and cerebral gray matter as shown in Fig. 2(a). In the adult human brain, the dura mater has a thickness of about 0.3 mm, while the thickness of the cerebral gray matter ranges from the L4 area to the surface of the cerebral cortex, approximately 0.8 mm [26].

To achieve optogenetic regulation, we choose two photosensitive proteins ChrimsonR [16] and C1V1 [23] that have been previously employed in visual optogenetic control. In Fig. 2(b), the excitation spectra of the two fluorescent proteins are presented together with the emission spectra of indium gallium phosphide (InGaP) red and indium gallium nitride (InGaN) green micro-LEDs fabricated in our laboratory [27], validating a correspondence between them. In order to compare which group of fluorescent proteins and micro-LEDs are more suitable for cortex prostheses, optical simulations are first conducted for wavelengths of 530 nm and 620 nm. To realize a high spatial resolution, the size of micro-LED is set to be 20 μm.

First, the ray tracing method (with the software TracePro [28]) is employed to numerically simulate the light propagation process with the brain tissue. The optical parameters applied in the simulation are presented in Table I [29], [30], [31], [32]. The normalized light intensity distributions along the propagation direction on the cross-sectional plane of the 530 nm and 620 nm wavelength cases based on the numerical simulation are depicted in Fig. 2(c) and (d). Then a mathematical model is developed to calculate analytical results to compare with the numerical results.

TABLE I
OPTICAL PARAMETERS USED IN SIMULATION

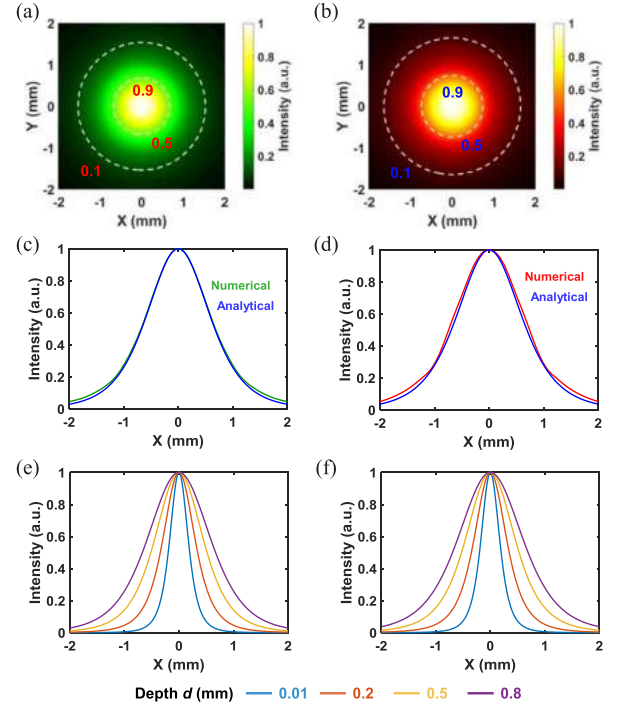| Materials	Absorption coefficient (/mm)	Scattering coefficient (/mm)	Anisotropy	Refractive Index
Gray matter of brain (530 nm) [28, 29]	0.104	32.8	0.861	1.36
Gray matter of brain (620 nm) [28, 29]	0.073	33.8	0.875	1.36
Dura (530 nm) [30, 31]	0.110	9.17	0.779	1.48
Dura (620 nm) [30, 31]	0.074	7.76	0.782	1.47

Fig. 3. (a) and (b) Top-viewed, normalized light intensity distribution profiles on L4 simulated at (a) 530 nm and (b) 620 nm. (c) and (d) Normalized light intensity distribution profiles along the horizontal direction on L4 At (c) 530 nm and (d) 620 nm. (e) and (f) Normalized light intensity distribution profiles along the horizontal direction at various depths (0.01, 0.2, 0.5 and 0.8 mm) in the brain, based on the analytical model At (e) 530 nm and (f) 620 nm.

In the mathematical model, the micro-LED is placed on the top of the dura matter and simplified as a Lambert light source. The light intensity received by a specific pixel in the tissue can be described as [33], [34]

$$I = I_0 \cos\theta \frac{\exp(-\mu_{\text{eff}}L)}{L^n} \tag{1}$$

Here I_0 represents the initial intensity of the light and θ is the angle between the direction of emitted light and the normal vector. L means the distance of light transmission. μ_{eff} is the effective attenuation coefficient and can be defined as

$$\mu_{\text{eff}} = \sqrt{\mu_{\text{a}}/D} \tag{2}$$

where μ_{a} is the absorption coefficient of the material, and D is the diffusion coefficient which can be defined as

$$D = \frac{1}{3[\mu_{\text{a}} + \mu_{\text{s}}(1-g)]} \tag{3}$$

where μ_{s} is the scattering coefficient of the material, and g is the anisotropy of the material.

In (1), n is a geometrical parameter depending on the propagation distance L. When L is smaller than the mean free path l, the transport process can be approximated by the wave theory where $n = 2$. When L is much larger than l, the transport process can be predicted via the diffusion theory where $n = 1$ [33], [34]. Here l can be defined as

$$l = \frac{1}{\mu_{\text{a}} + \mu_{\text{s}}(1-g)} \tag{4}$$

When calculating the variation curve of the light intensity received by a specific pixel along the normal direction with depth, we adopt a fixed value of $n = 1.2$ as an appropriate parameter for the consideration of normalization. Then the normalized light intensity analytical results varying with depth calculated by our model are compared with the numerical results simulated by the software in Fig. 2(e) and (f). The analytical results align well with the numerical results, which proves the reliability of the model.

Based on the simulation results, to achieve the threshold irradiances of 10 mW/mm^2 for C1V1 and ChrimsonR [35], [36], the optical power of one micro-LED should be 14.18 mW and 13.08 mW for green and red light. From the perspective of optical power, there is negligible difference between the two stimulation methods. However, there is a significant difference in the external quantum efficiency (EQE) between small-sized red and green micro-LEDs. The EQE of InGaN green and InGaP red micro-LEDs is about 15% and 5% respectively when the chip size is reduced to 20 μm [37]. The power of micro-LEDs for the stimulation of C1V1 and ChrimsonR should be 94.5 mW and 261.6 mW respectively. From a standpoint of energy consumption alone, opting for the stimulation scheme involving C1V1 and green micro-LEDs would be more suitable.

In addition to the intensity distributions along the propagation direction, the distributions on the receiving plane, which determine the resolution, are also of significant importance. Fig. 3(a) and (b) show the top-viewed normalized light intensity distribution profile on the L4 receiving plane for green and red illumination based on numerical simulation. To improve the accuracy of the model, n needs to vary with the depth d which represents the distance between light source and the receiving plane. Considering the wave theory and the diffusion theory combined, n can be described as

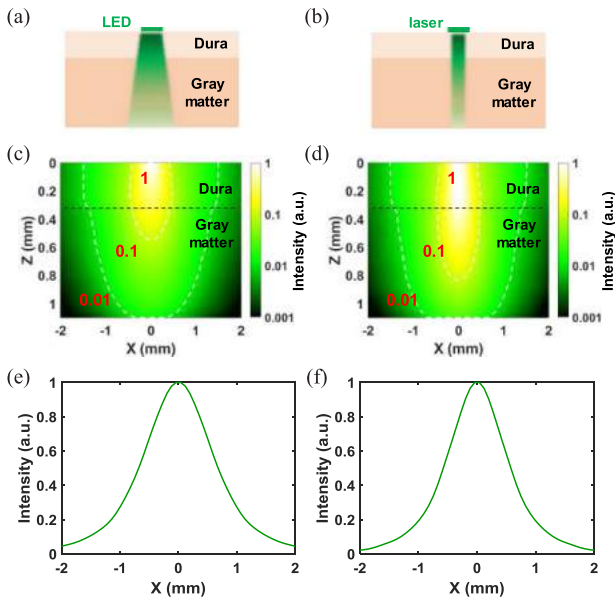$$n = 1 + \exp(-d/l) \tag{5}$$

Fig. 4.   (a) and (b) Optical models comparing optogenetic stimulation of the human visual cortex (V1) with (a) a green micro-LED and (b) a green laser. (c) and (d) Normalized light intensity distribution profiles on a cross-sectional plane along the propagation direction based on numerical simulation for (c) the micro-LED and (d) the laser. (e) and (f) Normalized light intensity distribution profiles along the horizontal direction on L4 for (e) the micro-LED and (f) the laser.

Fig. 5.   (a) and (b) Top-viewed, normalized light intensity distribution profiles on L4 (wavelength 530 nm) at distances (a) $\Delta x = 2$ mm and (b) $\Delta x = 1$ mm between two micro-LEDs. (c) and (d) Normalized light intensity distribution profile along the horizontal direction on L4 (wavelength 530 nm) at distances (c) $\Delta x = 2$ mm and (d) $\Delta x = 1$ mm . (e) Calculated resolution limits at varied depths in V1. (f) Schematic diagram of the micro-LED array (pitch = 1.3 mm) Displaying the character "E" of different sizes. (g) Schematic diagram the image received by L4 in V1.

The normalized light intensity distribution results along the horizontal direction on the L4 receiving plane at different wavelengths calculated by the analytical method are compared with the numerical results in Fig. 3(c) and (d) and demonstrate a high level of consistency. Then the normalized results at different depths in the gray matter for different colors are calculated in Fig. 3(e) and (f). As the penetration depth increases, the full width at half maximum (FWHM) of intensity peaks gradually increases, indicating a broaden distribution and reduced spatial resolutions. The FWHM values on the L4 layers for green and red situations reach about 1.36 mm and 1.48 mm. The small difference in FWHM between the two approaches suggests that there is a minimal discrepancy in resolution. In terms of comprehensive power consumption and horizontal distribution, stimulating C1V1 with green micro-LEDs is a more suitable scheme.

To determine the effects of different light sources on the spatial resolution, we compare the light distribution within V1 when utilizing a green micro-LED and a green laser device with the same geometry (Fig. 4). As shown in Fig. 4(a) and (b), the micro-LED is set as a Lambert source, while the laser emits parallel beam. The normalized light intensity distributions along the propagation direction on the cross-sectional plane for two different devices are simulated and depicted in Fig. 4(c) and (d). It can be seen that the laser source with parallel beam exhibits slightly improved penetration capability. Fig. 4(e) and (f) display the normalized intensity distribution profiles along the horizontal direction on L4. The FWHM value for the laser is 1.15 mm, which is only marginally better than that for the micro-LE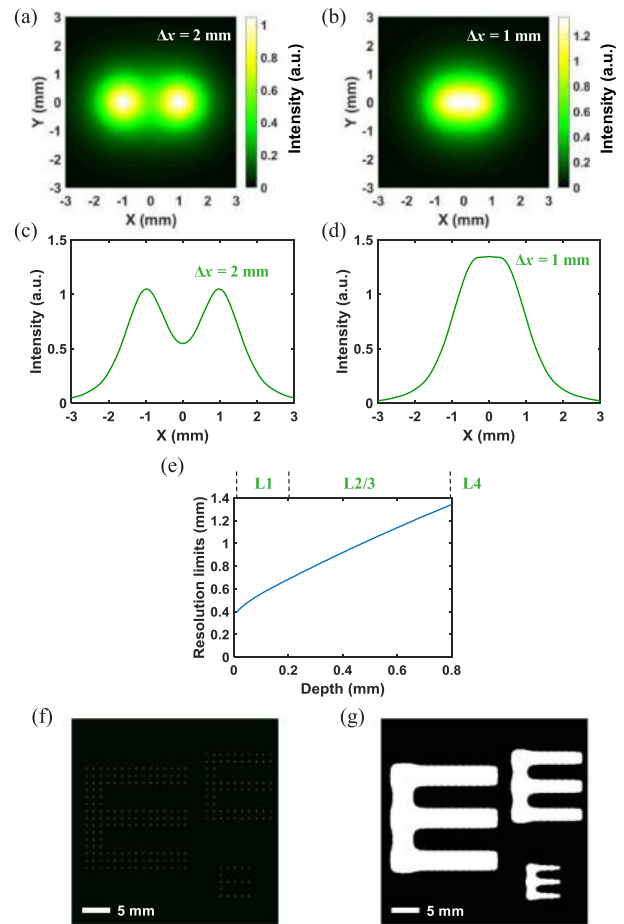D (1.36 mm). The resolutions for both devices remain within the millimeter range, indicating that the primary factor constraining the spatial resolution is the tissue scattering rather than the light source itself.

Utilizing the analytical model and the previously calculated horizontal distribution, we numerically predict the resolution limit of green micro-LED light irradiation. The resolution limit is the minimum distance between two adjacent micro-LEDs mounted on V1 that can distinguish two L4 receiving light spots, which implies that the secondary peak resulting from the overlap between the two spots is smaller in magnitude compared to the peak with the highest intensity. The receiving light spots herein refer to the positions with the highest intensity. Fig. 5(a)–(d) show the light intensity distribution results on the L4 for two adjacent micro-LEDs at various distances $\Delta x = 2$ mm and 1 mm. When the space Δx is 2 mm, two spots can be clearly distinguished. With the decrease of the space between two micro-LEDs, two spots are gradually overlapped. Two spots converge to form an indistinguishable spot when Δx is 1 mm. The resolution limit can be simplified as the FWHM, and the

TABLE II
THERMAL PARAMETERS USED IN SIMULATION

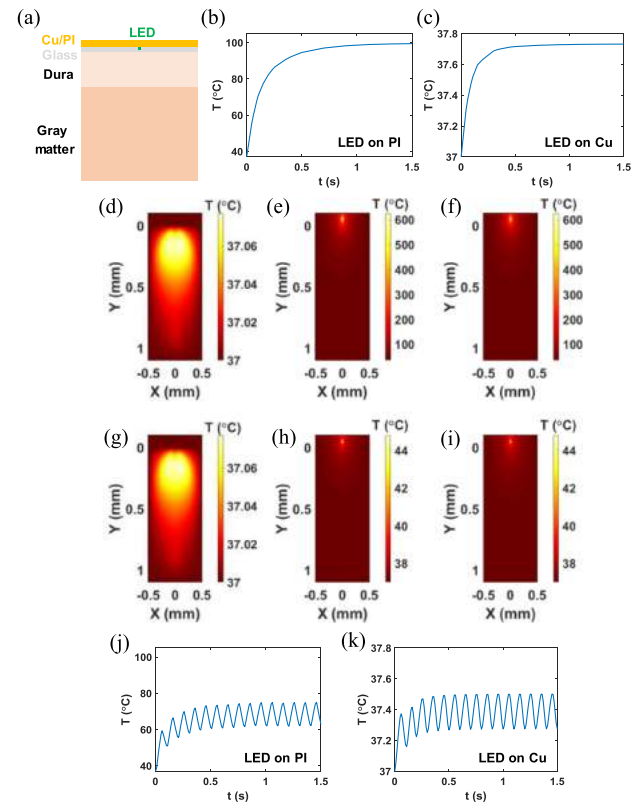| Material	Specific heat capacity (J/(kg·K))	Thermal conductivity (W/(m·K))	Density (kg/m^3)
Brain tissue	3650	0.5	1040
GaN	427	239	6149
Polyimide	766	0.837	1420
Cu	385	400	8960
Glass	730	1.4	2210

Fig. 6. (a) Cross-sectional view of the thermal model simulating the temperature distribution within the brain during LED operation. (b) and (c) Dynamic increases of the maximum temperature within the brain tissue when the micro-LED is turned on at t = 0 s. Here the micro-LED is mounted on (b) Polyimide (PI) or (c) Copper (Cu) substrates. (d–f) Steady-state temperature distribution with the device and the brain tissue, considering (d) the photothermal effect, (e) the electrothermal effect and (f) the combined effect when the substrate Is PI. (g–i) Steady-state temperature distribution with the device and the brain tissue, considering (g) the photothermal effect, (h) the electrothermal effect and (i) the combined effect when the substrate is Cu. (j) and (k) Dynamic increases of the maximum temperature within the brain tissue when a micro-LED operates in a pulsed mode (at a frequency of 10 Hz, duty cycle 0.5). Here the micro-LED is mounted on (j) Polyimide (PI) or (k) Copper (Cu) substrates.

resolution limit changed with the depth of the gray matter is shown in Fig. 5(e). In the ideal scenario, the peak intensity at the overlapping region between two micro-LEDs separated by the full FWHM is of equal to that of a single micro-LED. However, the overlap leads to an elevation in the peak value of the highest peak and a displacement towards the center. As a result, the actual resolution limit is slightly smaller than the FWHM. Based on the preceding discussion and analysis, it can be concluded that micro-LEDs with a spacing of approximately 1.3 mm can yield favorable resolution outcomes. Considering that the size of human primary visual cortex is about 4×4 cm^2 [38], the final array can consist of about 30×30 micro-LEDs. The schematic diagram of micro-LED array displaying different size characters "E" are presented in Fig. 5(f) and the corresponding image on the L4 is shown in Fig. 5(g). Through comparison, it becomes evident that the array is capable of forming distinct patterns and letters in the L4 region and verifies the feasibility of employing this array for visual restoration prostheses. It should be noted that here the micro-LED array is designed to target the L4. If we target more shallower regions like L2/3, the resolution limit can be further improved to ~0.8 mm (Fig. 5(e)).

Thermal simulations are also conducted to validate and optimize the design of the micro-LED array. As shown in Fig. 6(a), the thermal model is composed of the double-layer biological model developed above, a 50 μm thick glass layer, a 5 μm thick micro-LED with a size of 20 μm and a 50 μm thick substrate layer, which can be polyimide (PI) or copper (Cu). The thermal properties of these materials are presented in Table II. Then the transient and steady-state thermal distribution results are simulated through the finite-element analysis (COMSOL software) and the simulations are divided into two parts, the photothermal effect and the electrothermal effect. The photothermal effect is the heat solely caused by the optical irradiation, and the electrothermal effect is originated from the Joule heating from the electrically injected green micro-LED, which has a limited, non-unity EQE (~15%). Eventually, the temperature rise within the brain tissue is the combination of these two effects. We first apply polyimide tape as the soft substrate and observe the highest temperature within the tissue finally reaches about 100 °C (Fig. 6(b)). Comparing the photothermal and electrothermal results shown in Fig. 6(d) and (e), it can be found that the primary influencing factor lies in the device's heating and inadequate heat dissipation because of the poor thermal

conductivity of PI (0.837 W/m/K). To avoid the thermal damage, the material of the substrate is replaced by Cu, which has a much higher thermal conductivity (400 W/m/K). In this case, the highest temperature within the tissue is under 38 °C as shown in Fig. 6(c). The minimal disparity observed between Fig. 6(d) and (g) suggests that the substrate material has a negligible impact on the temperature increase induced by light radiation. More practically, pulsed stimulations are often used in optogenetics. In Fig. 6(j) and (k), we further analyze the thermal behaviors of micro-LEDs under pulsed operation (10 Hz frequency, 0.5 duty cycle). In this case, the temperature rise within the tissue is considerably lower than those captured under continuous illumination. Here we assume the green micro-LED has a fixed EQE (15%), independent of the operating temperature. When considering the thermal effect on the LED performance, the results for the devices on PI could be much worse. Thermal simulation results indicate that the micro-LED arrays necessitate the use of materials with high thermal conductivity like Cu as effective heat dissipation layers. For practical use, other metals

with better biocompatibilities, like titanium or platinum, can be considered.

III. Discussions

Based on the optical and thermal simulation, we design a micro-LED array as the optogenetic stimulator for visual cortical prostheses. InGaN green micro-LEDs for the stimulation for C1V1 are selected by comparing the power consumption and light distribution. The array is comprised of 30×30 micro-LEDs, with a precise spacing of 1.3 mm between each individual micro-LED considering the resolution limit. In order to mitigate potential thermal harm to biological tissues, it is imperative to incorporate a heat dissipation layer into the device design, given the small size of the components alongside their relatively high power consumption. The micro-LED array can theoretically be implanted on the dura mater to effectively stimulate the L4 region of the primary visual cortex with 900 channels, thereby fulfilling the requirements of an optogenetic visual cortical prosthesis.

The potential vision restoration effect achievable by the device can be roughly estimated by comparing the angular resolution of the human eye with the resolution of the device. In visual cortex close to the fovea, the cortical magnification is about 4 mm/° [39], which is estimated to achieve a final resolution of $0.325°$ and the corresponding visual acuity is 20/389. Although the performance is far from perfect when comparing with the normal human vision system (with a visual acuity of 20/20), the resulted effect is better than the Argus II of which the visual acuity can reach 20/1200 and can help the blind feel glowing objects or see patterns and characters. However, this estimation lacks accuracy as the precise mechanisms underlying the establishment of visual information in the visual cortex remain incompletely elucidated.

Resolution is a key determinant of the visual acuity attainable by the prosthesis, and the primary limiting factor in achieving high resolution is the significant scattering phenomenon within the tissue. Optical stimulation retinal prostheses can improve the resolution by increasing the numbers of stimulation channel. Notwithstanding, the L4 region is located at a specific depth within the cerebral cortex, distinct from photoreceptors that reside on the surface of the retina. The scattering phenomenon encountered during the penetration process imposes a resolution limit in the millimeter range, and solely increasing the number of channels does not effectively enhance the final resolution. To overcome the challenge, a Utah optrode array permit focal optogenetic stimulation of deep layer neurons [40]. The device with the size of 4×4 mm^2 consisted of 10×10 glass needle waveguides bonded to an addressable micro-LED array and was validated to achieve sub-millimeter level stimulation in macaque primary visual cortex. The specifically engineered waveguides can effectively mitigate light scattering within tissues, but they may also pose a potential risk of mechanical damage to the tissue. Advancing resolution capabilities to enhance restored visual acuity while concurrently preserving the benefits of minimal tissue damage is the subsequent objective of optogenetic visual cortical prostheses.

IV. Summary

In this paper, we first review the recent progress on the development of various visual prostheses. Based on the stimulation position, visual prostheses can be divided into retina prostheses and visual cortical prostheses. The prostheses for retina can replace photoreceptors and treat relevant diseases like AMD and RP. Relatively, visual cortical prostheses can directly active higher level neurons and are indicated for the management of more intricate and severe visual impairments. Based on the stimulation mode, the prostheses can be divided into electrical stimulators and optogenetic stimulators. The electrical strategy is characterized by its maturity and gene-independent nature, and the optogenetic strategy presents advantages of cell specificity, reduced tissue damage and theoretically better spatial resolution.

To achieve high-density optical stimulation of the visual cortex, we design a micro-LED array for visual cortical prostheses. Through optical modeling calculations and software simulations, we conduct a comparative analysis of the power consumption requirements and resolution between two distinct optogenetic approaches, separately utilizing C1V1 and ChrimsonR. Following meticulous evaluation, the method of utilizing green light for the activation of C1V1 is recommended, based on the state-of-the-art micro-LED technologies. The spacing for individual devices and number of channels in the array are determined by calculating the optical field distribution and resolution limit. The design of the device's heat dissipation layer is optimized through thermal simulations to ensure that it does not cause any thermal damage to the tissues. We perform simulations to assess both the display performance of the array and the activation effects within the designated stimulation area, verifying the feasibility of the design in visual cortical prostheses.

Finally, we discuss the visual efficacy attainable through the utilization of this visual prosthesis and the primary factors that constrain the resolution of optical stimulation for visual cortex, specifically the L4 in V1. The resolution is hindered by scattering within the tissue, and the potential solution Utah optrode array is also introduced. Currently, further advancements in the application of optical visual cortical prostheses are still pending, as the challenges of severe scattering within tissues and the elucidation of biological visual signal mechanisms need to be addressed.

References

[1] J. Cehajic-Kapetanovic, M. S. Singh, E. Zrenner, and R. E. MacLaren, "Bioengineering strategies for restoring vision," *Nature Biomed. Eng.*, vol. 7, no. 4, pp. 387–404, 2023.

[2] G. M. Acland et al., "Gene therapy restores vision in a canine model of childhood blindness," *Nature Genet.*, vol. 28, no. 1, pp. 92–95, 2001.

[3] J. W. B. Bainbridge et al., "Effect of gene therapy on visual function in Leber's congenital amaurosis," *New England J. Med.*, vol. 358, no. 21, pp. 2231–2239, 2008.

[4] D. A. Lamba, J. Gust, and T. A. Reh, "Transplantation of human embryonic stem cell-derived photoreceptors restores some visual function in Crx-deficient mice," *Cell Stem Cell*, vol. 4, no. 1, pp. 73–79, 2009.

[5] M. S. Singh and R. E. MacLaren, "Stem cells as a therapeutic tool for the blind: Biology and future prospects," *Proc. Roy. Soc. B: Biol. Sci.*, vol. 278, no. 1721, pp. 3009–3016, 2011.

[6] J. Ribeiro et al., "Restoration of visual function in advanced disease after transplantation of purified human pluripotent stem cell-derived cone photoreceptors," *Cell Rep.*, vol. 35, no. 3, 2021, Art. no. 109022.

[7] J. D. Steinmetz et al., "Causes of blindness and vision impairment in 2020 and trends over 30 years, and prevalence of avoidable blindness in relation to VISION 2020: The Right to Sight: An analysis for the Global Burden of Disease Study," *Lancet Glob. Health*, vol. 9, no. 2, pp. e144–e160, 2021.

[8] K. Y. Wu, M. Mina, J.-Y. Sahyoun, A. Kalevar, and S. D. Tran, "Retinal prostheses: Engineering and clinical perspectives for vision restoration," *Sensors*, vol. 23, no. 13, 2023, Art. no. 5782.

[9] Y. H.-L. Luo and L. da Cruz, "The Argus II Retinal prosthesis System," *Prog. Retinal Eye Res.*, vol. 50, pp. 89–107, 2016.

[10] E. Zrenner et al., "Subretinal electronic chips allow blind patients to read letters and combine them to words," *Proc. Roy. Soc. B: Biol. Sci.*, vol. 278, no. 1711, pp. 1489–1497, 2010.

[11] J. Tang et al., "Nanowire arrays restore vision in blind mice," *Nature Commun.*, vol. 9, no. 1, 2018, Art. no. 786.

[12] D. Palanker, Y. L. Mer, S. Mohand-Said, M. Muqit, and J. A. Sahel, "Photovoltaic restoration of central vision in atrophic age-related macular degeneration," *Ophthalmology*, vol. 127, no. 8, pp. 1097–1104, 2020.

[13] F. Zhang et al., "Multimodal fast optical interrogation of neural circuitry," *Nature*, vol. 446, no. 7136, pp. 633–639, 2007.

[14] S. N. Obaid et al., "Flexible electro-optical arrays for simultaneous multi-site colocalized spatiotemporal cardiac mapping and modulation," *Adv. Opt. Mater.*, vol. 10, no. 23, 2022, Art. no. 2201331.

[15] E. K. Knudsen et al., "A thin-film optogenetic visual prosthesis," 2023, *bioRxiv:2023.01.31.526482*.

[16] A. Soltan et al., "A head mounted device stimulator for optogenetic retinal prosthesis," *J. Neural Eng.*, vol. 15, no. 6, 2018, Art. no. 065002.

[17] X. Chen, F. Wang, E. Fernandez, and P. R. Roelfsema, "Shape perception via a high-channel-count neuroprosthesis in monkey visual cortex," *Science*, vol. 370, no. 6521, pp. 1191–1196, 2020.

[18] S. Niketeghad and N. Pouratian, "Brain machine interfaces for vision restoration: The current State of cortical visual prosthetics," *Neurotherapeutics*, vol. 16, no. 1, pp. 134–143, 2019.

[19] P. R. Troyk, "The Intracortical Visual Prosthesis Project," in *Artificial Vision: A Clinical Guide*, V. P. Gabel Ed. Cham, Switzerland: Springer, 2017, pp. 203–214.

[20] E. Fernández and R. A. Normann, "CORTIVIS approach for an intracortical visual prostheses," in *Artificial Vision: A Clinical Guide*, V. P. Gabel Ed. Cham, Switzerland: Springer, 2017, pp. 191–201.

[21] A. Szelényi, B. Joksimovic, and V. Seifert, "Intraoperative risk of seizures associated with transient direct cortical stimulation in patients with symptomatic epilepsy," *J. Clin. Neurophysiol.*, vol. 24, no. 1, pp. 39–43, 2007.

[22] J. P. Lefaucheur, "Methods of therapeutic cortical stimulation," *Neurophysiologie Clinique/Clin. Neurophysiol.*, vol. 39, no. 1, pp. 1–14, 2009.

[23] R. Rajalingham et al., "Chronically implantable LED arrays for behavioral optogenetics in primates," *Nature Methods*, vol. 18, no. 9, pp. 1112–1116, 2021.

[24] W. Sun, Z. Tan, B. D. Mensh, and N. Ji, "Thalamus provides layer 4 of primary visual cortex with orientation- and direction-tuned inputs," *Nature Neurosci.*, vol. 19, no. 2, pp. 308–315, 2016.

[25] R. J. Douglas and K. A. C. Martin, "Neuronal circuits of the neocortex," *Annu. Rev. Neurosci.*, vol. 27, no. 1, pp. 419–451, 2004.

[26] E. G. Jones, "Microcolumns in the cerebral cortex," *Proc. Nat. Acad. Sci.*, vol. 97, no. 10, pp. 5019–5021, 2000.

[27] L. Li et al., "Transfer-printed, tandem microscale light-emitting diodes for full-color displays," *Proc. Nat. Acad. Sci.*, vol. 118, no. 18, 2021, Art. no. e2023436118.

[28] X. Cai et al., "A dual-channel optogenetic stimulator selectively modulates distinct defensive behaviors," *iScience*, vol. 25, no. 1, 2022, Art. no. 103681.

[29] S. C. Gebhart, W. C. Lin, and A. Mahadevan-Jansen, "In vitro determination of normal and neoplastic human brain tissue optical properties using inverse adding-doubling," *Phys. Med. Biol.*, vol. 51, no. 8, 2006, Art. no. 2011.

[30] S. Alaa, N. L. Ekaterina, and V. T. Valery, "Measurement of the refractive index of the gray matter of the cow's brain at wavelengths of 480-1550 nm when exposed to different temperatures," *Proc. SPIE*, vol. 12192, pp. 221–235, 2022.

[31] N. B. Alexey et al., "In-vitro study of control of human dura mater optical properties by acting of osmotical liquids," *Proc. SPIE*, vol. 4162, pp. 182–188, 2000.

[32] A. N. Bashkatov et al., "Glucose and mannitol diffusion in human dura mater," *Biophysical J.*, vol. 85, no. 5, pp. 3310–3318, 2003.

[33] R. Nazempour, C. Liu, Y. Chen, C. Ma, and X. Sheng, "Performance evaluation of an implantable sensor for deep brain imaging: An analytical investigation," *Opt. Mater. Exp.*, vol. 9, no. 9, pp. 3729–3737, 2019.

[34] L. V. Wang and H.-I. Wu, *Biomedical Optics: Principles and Imaging*. Hoboken, NJ, USA: Wiley, 2012.

[35] N. C. Klapoetke et al., "Independent optical excitation of distinct neural populations," *Nature Methods*, vol. 11, no. 3, pp. 338–346, 2014.

[36] M. Prigge et al., "Color-tuned channelrhodopsins for multiwavelength optogenetics," *J. Biol. Chem.*, vol. 287, pp. 31804–31812, 2012.

[37] E.-L. Hsiang et al., "Improving the power efficiency of micro-LED displays with optimized LED chip sizes," *Crystals*, vol. 10, 2020, Art. no. 494.

[38] E. C. Bush and J. M. Allman, "Three-dimensional structure and evolution of primate primary visual cortex," *Anat. Rec. Part A: Discoveries Mol., Cellular, Evol. Biol.*, vol. 281A, no. 1, pp. 1088–1094, 2004.

[39] A. Cowey and E. T. Rolls, "Human cortical magnification factor and its relation to visual acuity," *Exp. Brain Res.*, vol. 21, no. 5, pp. 447–454, 1974.

[40] A. M. Clark et al., "An optrode array for spatiotemporally precise large-scale optogenetic stimulation of deep cortical layers in non-human primates," 2022, *bioRxiv:2022.02.09.479779*.

Junyu Chen received the B.Eng. degree in 2022 from the Department of Electronic Engineering, Tsinghua University, Beijing, China, where he is currently working toward the Ph.D. degree.

He Ding received the Ph.D. degree from Ecole Centrale de Lyon, France, in 2016, and the Postdoctoral studies from Tsinghua University, Beijing, China, from 2016 to 2018.

He is currently an Assistant Professor with the School of Optics and Photonics, Beijing Institute of Technology, Beijing.

Ya-tang Li received the Ph.D. degree from the University of Southern California, Los Angeles, CA, USA. He completed the postdoctoral training from the California Institute of Technology, Pasadena, CA, USA.

He is currently an Assistant Investigator with the Chinese Institute for Brain Research, Beijing, China.

Xing Sheng received the B.Eng. degree from Tsinghua University, Beijing, China, in 2007, and the Ph.D. degree from the Massachusetts Institute of Technology, Cambridge, MA, USA, in 2012. He is currently an endowed Associate Professor with the Department of Electronic Engineering, Tsinghua University.